Int. J. Electrochem. Sci., 4 (**2009**) 820 - 831

International Journal of ELECTROCHEMICAL SCIENCE
www.electrochemsci.org

Corrosion Resistance and Mechanical Properties of an Al 9wt%Si Alloy Treated by Laser Surface Remelting

Wislei R. Osório [*], Noé Cheung, Leandro C. Peixoto and Amauri Garcia [**]

Department of Materials Engineering, University of Campinas, UNICAMP, P.O. Box 6122, 13083 – 970 Campinas, SP, Brazil
[*]E-mail: wislei@fem.unicamp.br
[**]E-mail: amaurig@fem.unicamp.br

Received: 6 April 2009 / *Accepted:* 11 May 2009 / *Published:* 6 June 2009

The correlation of corrosion behavior and mechanical properties with microstructure parameters can be very useful for planning solidification conditions in order to achieve a desired level of final properties. The aim of the present work is to investigate the influence of microstructural array parameters of as-cast and laser remelted Al-9 wt% Si alloy samples on the resulting mechanical properties and the electrochemical behavior. As-cast samples were obtained with two different cooling rates and surface remelted samples by laser were obtained with a continuous CO_2 laser. Electrochemical impedance spectroscopy (EIS) technique and Tafel's plots in a 0.5M NaCl test solution at 25˚C were carried out. An equivalent circuit has also been proposed and impedance parameters have been simulated by the Zview® software. Laser surface remelting (LSR) have induced microstructural morphologies typified by highly branched fine silicon fibers with a deleterious effect on the electrochemical corrosion resistance.

Keywords: As-cast microstructure, Mechanical properties, Dendrite arm spacing, Corrosion behaviour, Laser remelting

1. INTRODUCTION

The effect of microstructure on metallic alloys properties has been highlighted in various studies, particularly the influence of dendrite arm spacing on mechanical properties and corrosion behavior relationships [1-4]. Aluminum castings have played an integral role in the growth of the aluminum industry since its inception in the late 19th century. Silicon is the main alloying element; it imparts high fluidity and low shrinkage, which results in good castability and weldability [5]. Aluminum alloys with silicon as a major alloying element constitute a class of material, which provides the most significant part of all shaped castings manufactured, having a wide range of applications in the automotive and aerospace industries [6]. This is mainly due to the outstanding effect of silicon in the improvement of casting characteristics, combined with other physical properties such as mechanical properties and corrosion resistance.

Aluminum-silicon alloys can have the mechanical properties significantly improved by structural modification in the normally occurring eutectic. In general, the greatest benefits are achieved in alloys containing from 5wt% Si up to the eutectic concentration. Mechanical properties of Al–Si casting alloys depend not only on their chemical composition but are also significantly dependent on microstructural features such as the morphologies of the Al-rich α-phase and of the eutectic Si particles [5-6]. Typical hypoeutectic aluminum-silicon alloys have two major microstructural components, namely primary aluminum and an aluminum-silicon eutectic. For metal-non-metal eutectics the growth form of the faceting phase (Si) is such as to produce a three-dimensional skeletal crystal pattern rather than thin sheets. Although the silicon plates appear to be separated crystals they are in fact interconnected. Eutectic Si in as-cast Al–Si foundry alloys has often a very coarse and plate-like morphology, leading to poor mechanical properties, particularly ductility [7].

Laser surface treatments are an efficient means of local transformations of mechanical and chemical properties. The cleanliness, the speed and the automation inherent to the laser process are also factors in making laser applications extremely competitive in an industrial environment [8-10]. Very fast heat extraction during solidification results in very high cooling rates of about 10^5-10^8 $^oC/s$ when a laser surface remelting (LSR) is applied [11, 12]. The microstructures of rapidly solidified materials show advantages of refinement, reduced microsegregation, extended solid solubility and formation of metastable phases [13, 14].

To date, few researches have been conducted regarding to the corrosion behavior of LSR Al-Si alloys. Further, contradictory results were found and no satisfactory explanations have been provided by the existing studies [15-20], in particular concerning the relationship between microstructures and electrochemical responses. For instance, Opera et al. [16] have reported a decrease on the corrosion resistance for a LSR Al-Si alloy tested in a 5% NaCl solution. In contrast, Wong and Liang [17, 18] have found that the laser remelting process had no significant effect on the corrosion behavior of different Al-Si alloys (6, 10 and 13 wt% Si), also tested in a 5% NaCl solution.

There exists a great preoccupation with corrosion effects on a number of materials. There are attempts to combine theory and practical experience from investigations of a number of substances in order to find models to predict the corrosion and to report experimental corrosion behavior or synthesized compounds to act as corrosion inhibitors [21-21].

Recent articles on Al-Si alloys have reported that coarser dendritic structures yield higher corrosion resistance than finer dendritic structures, and that this is associated with the morphology of the interdendritic eutectic mixture [19-20]. It was also reported that the silicon content is another important parameter affecting mechanical and corrosion resistances [20]. Osorio et al. [12] have recently reported that the laser surface remelting process provided a significant microstructural refinement and decreased the corrosion resistance in sulphuric acid and sodium chloride solutions.

The aim of this paper was to analyze the role of the resulting microstructure on the mechanical properties and the general corrosion resistance of LSR and as-cast Al-9wt% Si alloy samples tested in a 0.5M NaCl solution at 25^{o}C. Experimental results include dendrite arm spacings (λ_2), ultimate tensile strength (σ_u), yield strength (σ_y), corrosion potential (E_{Corr}), corrosion current density (i), polarization resistance (R_1), and capacitances values (Z_{CPE}).

2. EXPERIMENTAL

The Al-9wt%Si alloy was prepared from commercially pure metals: Al (99.72wt%) and Si (99.58wt%). The mean impurities were Fe (0.08%), Cu (0.02%) and Pb (0.001%), and other with concentration less than 50 ppm.

A permanent low-carbon steel (SAE 1020) mold with an internal diameter of 50 mm, height 50 mm and a 3 mm wall thickness was used to obtain as-cast samples. Initially, the Al-9wt%Si alloy was melted in an electric resistance-type furnace until the molten alloy reached a predetermined temperature (at about 10% above the liquidus temperature, 660 ^oC). It was then stirred, degassed and poured into the casting chamber (permanent low-carbon steel mold at two different temperatures of about: 25 ^oC and 250 ^oC, in order to provide different range of cooling rates). This procedure yielded cooling rates in a range of about 8 to 12 $^oC/s$ and 2 to 4 $^oC/s$, respectively. Temperatures were monitored via type J thermocouples (sheathed in 1.6mm outside diameter stainless steel protection tubes).

Al-9wt%Si alloy samples have been subjected to LSR by using a continuous CO_2 laser delivering a nominal output power of 1 kW. Before laser treatment, the samples were sandblasted in order to ensure uniform surface finishing. The samples have been coated with graphite to produce blackned surfaces in order to increase absorptivity, and were then scanned at a laser beam speed of 1000 mm/min with defocused beam (radius = 0.6 mm). The cooling rate during LSR attained values in a range from 2000 to 3000 $^oC/s$.

As-cast and laser treated specimens were sectioned, ground, polished and etched by using a 0.5 %HF solution at room temperature for microscopy examination. The microstructural characterization was carried out by using an optical microscopy associated with an image processing system Neophot 32 (Carl Zeiss, Esslingen, Germany) and Leica Quantimet 500 MC (Leica Imaging Systems Ltd, Cambridge, England). X-ray diffraction (XRD) measurements were carried out in both as-cast and laser treated specimens in order to verify microstructural and phases modifications at their surfaces. X-ray diffraction patterns were obtained utilizing CuK α radiation with a wavelength, λ, of 0.15406 nm.

The tensile tests were performed according to specifications of ASTM Standard E 8M. In order to provide average values of ultimate tensile and yield strengths, three specimens were tested for each condition (as-cast). Average values of Vickers hardness were also obtained from triplicate specimens.

In order to evaluate the electrochemical corrosion behavior of the Al-9wt%Si alloy samples, electrochemical corrosion tests were performed in a 1cm^2 circular area of ground (600 grit SiC finish) sample surfaces. Electrochemical impedance spectroscopy (EIS) measurements began after an initial delay of 30 minutes for the samples to reach a steady-state condition. The tests were carried out with the samples immersed in a stagnant and naturally aerated 500 cm^3 of a 0.5 M NaCl solution at 25 ºC under a pH of about 6.8 (±0.5). A potentiostat (EG & G Princeton Applied Research, model 273A) coupled to a frequency analyzer system (Solartron model 1250), a glass corrosion cell kit with a platinum counter-electrode and a saturated calomel reference electrode (SCE) were used to perform the EIS tests. The potential amplitude was set to 10 mV, peak-to-peak (AC signal), with 5 points per decade and the frequency range was set from 100 mHz to 100 kHz. The samples were further ground to a 1200 grit SiC finish, followed by distilled water washing and air drying before measurements. Potentiodynamic measurements were also carried out in the aforementioned solution at 25 ^{o}C using a potentiostat at the same positions where the EIS tests were carried out. Using an automatic data acquisition system, the potentiodynamic polarization curves were plotted and both corrosion rate and potential were estimated by Tafel plots by using both anodic and cathodic branches at a scan rate of 0.2 mV s^{-1} from -250 mV (SCE) to +250 mV (SCE). Duplicate tests for EIS and potentiodynamic polarization curves were carried out. In order to supply quantitative support for discussions of these experimental EIS results, an appropriate model (ZView version 2.1b) for equivalent circuit quantification has also been used. Impedance parameters such as polarization resistances and capacitances were obtained by using the equivalent circuit technique.

3. RESULTS AND DISCUSSION

3.1. Microstructure

Typical resulting microstructures for as-cast and laser remelted Al-9wt%Si samples are shown in Fig.1. The as-cast sample has a microstructure characterized by an Al-rich dendritic matrix (α-Al phase) and a eutectic mixture in the interdendritic region formed by silicon particles, which are coarse and distributed in a plate-like morphology, set in an Al-rich phase, as shown in Fig. 1(a) and (b). The microstructural pattern of laser treated samples is shown in Fig. 1(c). It is clearly observed that the resulting remelted zone exhibits a very refined microstructure. Neither porosity nor cracks have been observed on the treated surface. It is well known that the dendritic refinement improves mechanical properties [19-20, 23-24]. Comparisons between as-cast and laser remelted microstructures permit to observe a significant dendritic refinement. As-cast (cooling rates of about 10 ^{o}C/s and 3^{o}C/s) and laser remelted (2000 ^{o}C/s) samples have secondary dendrite arm spacings of about 35 μm, 15 μm and 2.5 μm, respectively. White and dark regions are, the Al-rich dendritic matrix and the Si-rich interdendritic region (eutectic mixture), respectively. Particularly, for Al-Si castings, it is well known that smaller dendritic arm spacings are associated with a more extensive distribution of silicon particles in the

Al-9wt%Si (As-cast) λ_2 = 35 µm **Eutectic**: angular plate-like silicon particles (width: 5.0µm) **Etchant:** 0.5%HF solution **(a)**	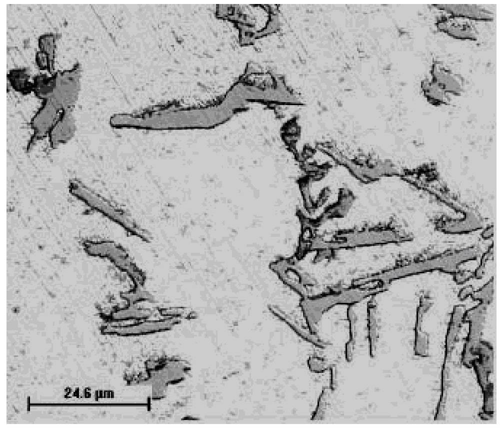
Al-9wt%Si (As-cast) λ_2 = 15 µm **Eutectic**: angular plate-like silicon particles (width: 5.0µm) **Etchant:** 0.5%HF solution **(b)**	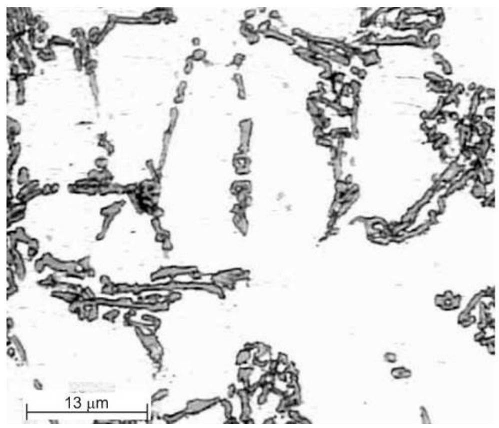
Al-9wt%Si (Remelted) λ_2 = 2.5 µm **Eutectic**: angular plate-like silicon particles (width: 5.0µm) **Etchant:** 0.5%HF solution **(c)**	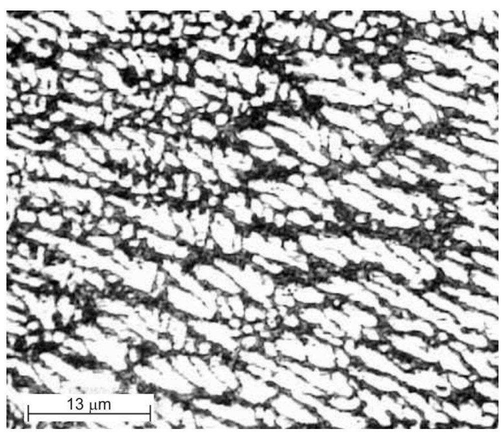

Figure 1. Microstructures of cross sections of Al-9wt% Si alloy: (a) as-cast (cooling rate: 2 to 4 $^oC/s$), (b) as-cast (cooling rate: 8 to 12 $^oC/s$) and (c) laser remelted (cooling rate: 2 10^3 to 3 10^3 $^oC/s$).

interdendritic regions and thus contributing to the increase in tensile strength [19-20]. The laser treatment has provided an effective refinement on the Al-9wt%Si alloy samples with pool depth of about 400 µm and pool width of about 900 µm in each laser track, as also reported by Osório et al. [12]. It is important to remark that remelted samples were obtained in the center of the remelted track.

It is known that in the overlap zone, a coarser structure is developed due to the lower solidification speed when compared to those of the other treated regions [12]. A peak associated to the silicon-rich phase at about 65 degrees can be observed in the X-ray diffraction patterns for as-cast and remelted Al 9wt% Si alloy samples. The LSR process has induced precipitation of Si into the Al-rich dendritic matrix, as also reported by Wong and Liang [17, 18].

3.2. Mechanical properties

In the as-cast and laser remelted conditons the specimens have significant variations in the resulting microstructures. Thus, it is also expected that such microstructural changes provoke differences on the final mechanical properties. Table 1 presents the experimental results of ultimate tensile strength (UTS), yield strength (YS: 0.2 % proof stress), elongation (δ) and Vickers hardness (HV) for as-cast Al-9wt%Si alloy samples. For the laser treated sample, the UTS, YS and δ were obtained from correlations between secondary dendrite arm spacing and mechanical properties [12, 19, 24]. The results of UTS, YS and HV for as-cast and laser treated conditions are consistent with those found in the literature concerning Al-Si commercial casting alloys [19, 23-24].

Table 1. Ultimate and yield tensile strengths (UTS and YS), elongation (δ), Vickers hardness (HV) and secondary dendrite arm spacing (λ_2) of as-cast and heat-treated samples.

Sample	UTS (MPa)	YS (MPa)	δ (%)	HV	λ_2(μm)
As-cast (2 to 4 ^{o}C/s)	142 (122-148)	65 (62-68)	8 (7-9)	72 (64-75)	35 (30-39)
As-cast (8 to 12 ^{o}C/s)	165 (150-188)	72 (65-88)	6 (5-7)	82 (80-91)	15 (13-18)
Laser Remelted (2 10^3 to 3 10^3 ^{o}C/s)	306 (288-315)	102 (96- 105)	3 (2-5)	120 (100-130)	2.5 (2-3)

Numbers in parentheses represent maximum and minimum values.

The tendency of enhance on UTS presented by the refined alloy samples seems to be associated with an increase of obstacles to slip due to the more extensive distribution of α-Al phase/ fibrous silicon particles boundaries. It is important to remark that the dendrite array has an important role on mechanical properties, particularly in the UTS, as recently reported [1-6, 24]. By comparing the corresponding results for as-cast and laser remelted Al-9wt%Si samples, it can be seen that the latter exhibits a significant improvement in UTS and HV.

Equations correlating dendritic array and mechanical properties are reported [19, 24]. These equations can incorporate dendritic growth models expressing λ_2 as a function of thermal solidification variables permitting expressions correlating mechanical properties with solidification conditions to be established [19, 24]. Fig.3 shows a comparison between experimental and simulated results concerning EIS diagrams in Bode-phase and Nyquist plots for as-cast and laser remelted Al-9%Si alloy samples.

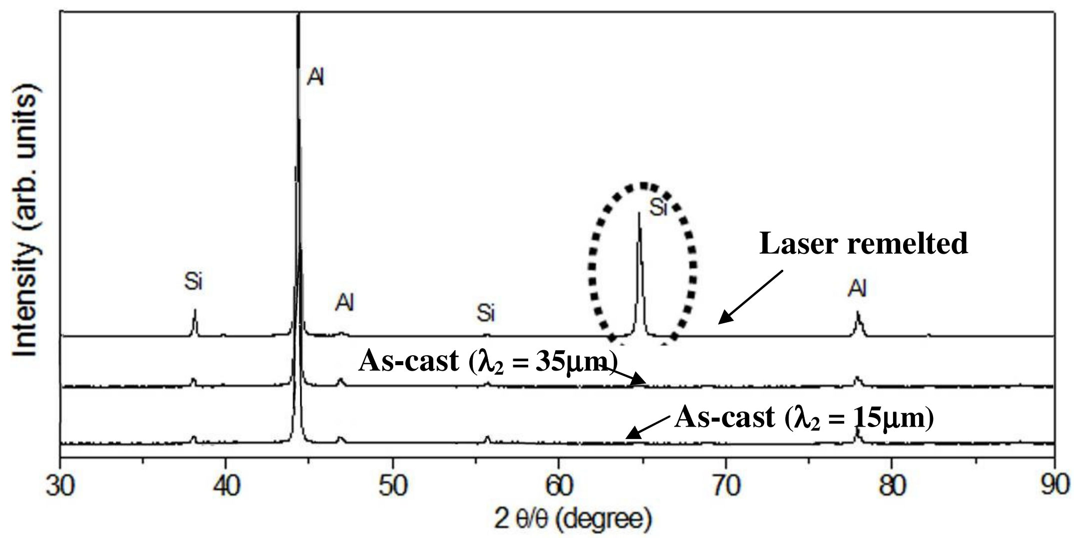

Figure 2. Typical XRD patterns for laser remelted and as-cast Al 9wt% Si alloy samples.

For the laser remelted sample, the maximum phase angle is associated with a displacement of about one decade in frequency (at 1 Hz) and its correspondent diameter of the capacitive arc (Nyquist plots) is considerable decreased when compared with the corresponding results of the as-cast samples, as shown in the Bode-phase and Nyquist plots. Such behavior is a reasonable indication of a decrease on the corrosion resistance of the Al9wt%Si laser remelted sample. The equivalent circuit and impedance parameters are shown in Fig. 4 and Table 2, respectively.

The proposed circuit was chosen due to the best fitting quality with the experimental data [5, 12, 20, 24, 25]. The fitting quality was evaluated by chi-squared (χ^2) values of about 10^{-3}~10^{-4}, which were interpreted by the ZView software and are also shown in Table 2. It can be seen that the LSR process has increased significantly the capacitance $Z_{CPE(1)}$ associated to a decrease in both resistances R_1 and R_2, compared with the corresponding values of the as-cast samples. Such tendency of results can be associated with a deleterious effect on the corrosion resistance of the Al9wt%Si laser treated alloy [26-27]. In order to understand the physical significance of each element of the electronic equivalent circuit, it can be considered that R_{el} corresponds to the electrolyte resistance, R_1 and R_2 correspond to the polarization resistance of the surface of the samples and oxide film formations, respectively. The $Z_{CPE(1)}$ and $Z_{CPE(2)}$ correspond to the capacitances (at 1Hz < F < 1kHz) of the experimentally examined samples and their oxide layer formation, respectively. The Z_{CPE} generally denotes the impedance of a phase element as $Z_{CPE} = [\ C\ (j\ w)^{\ n}\ ]^{-1}$[5, 12, 20, 24]. The parameters n_1 and n_2 are correlated to the phase angle, varying between -1 and 1.

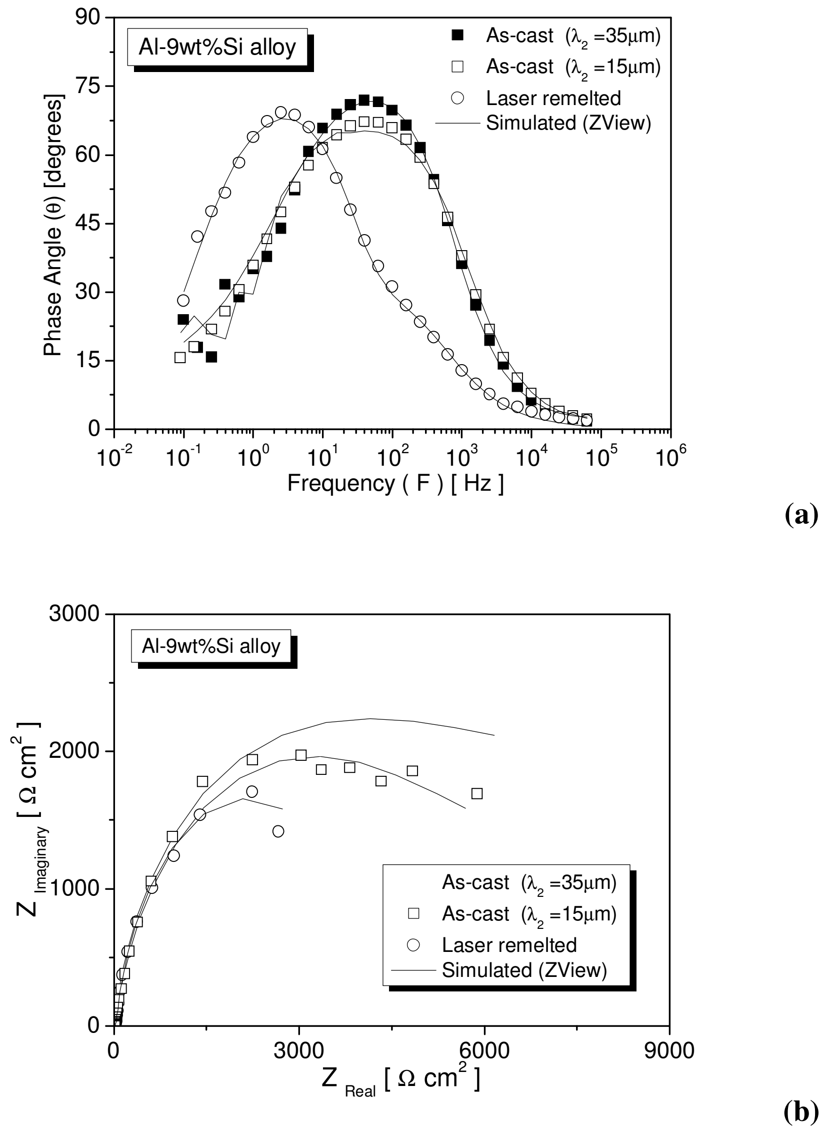

Figure 3. Experimental and simulated EIS diagrams obtained by the ZView® software: (a) Bode-phase and (b) Nyquist plots for Al–9 wt%Si samples in a 0.5 M NaCl solution at 25 °C.

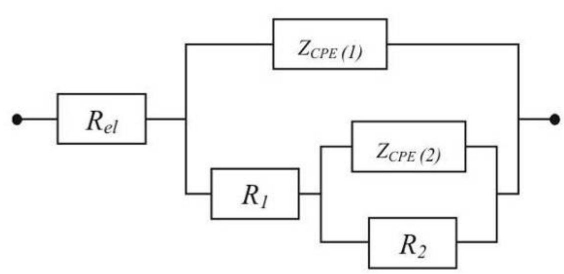

Figure 4. Proposed equivalent circuit used to obtain impedance parameters by using ZView ®.

Table 2. Impedance parameters of Al-9wt%Si as-cast (AC1) with λ_2 =35μm, as-cast (AC2) with λ_2 =15μm and laser remelted (LR) samples in a 0.5M NaCl solution at 25°C obtained from ZView® software.

Parameters	As-cast (AC1)	As-cast (AC2)	Laser remelted (LR)
R_{el} (Ω cm^2)	20.13	20	21
$Z_{CPE\ (1)}$ (μF cm^{-2})	41 (±5)	43 (±3)	176 (±10)
$Z_{CPE\ (2)}$ (μF cm^{-2})	820 (±5)	200 (±20)	75 (±5)
n_1	0.80	0.80	0.78
n_2	0.78	0.95	0.97
R_1 (Ω cm^2)	5250	2250	60
R_2 (Ω cm^2)	2 10^{15}	15000	4275
χ^2	46 10^{-4}	25 10^{-3}	23 10^{-4}

Potentiodynamic polarization curves for as-cast and laser remelted Al-9wt% Si alloy samples in 0.5M NaCl solution at 25 °C are shown in Fig. 5. Such results permit to reinforce the corrosion resistance tendency which has been observed when analyzing experimental and simulated Bode-phase and Nyquist plots for the Al9wt%Si alloy, with the LSR samples providing higher corrosion rate. Although laser surface remelting has increased the corrosion current density (of about 2 μA cm^{-2}) when compared to the results of the as-cast samples, a considerable displacement on the corrosion potential towards the nobler side (at -700mV, SCE) can be observed. The shapes of the cathodic and anodic branches of the as-cast Al-9wt% Si alloy sample characterize typical pitting reactions, differently to that exhibited for the laser remelted sample, as shown in Fig. 5.

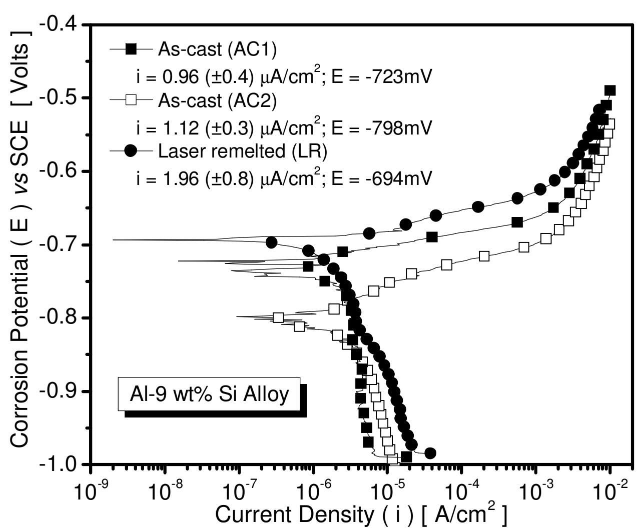

Figure 5. Potentiodynamic polarization curves of Al-9wt%Si alloy samples tested in 0.5M NaCl solution at 25°C.

Although the microstructural refinement is hardly desired by major foundry industries in order to increase the mechanical properties, the corrosion resistance can be significantly affected. The aforementioned experimental and simulated impedance parameters provide sufficient information to conclude that the use of the laser surface remelting treatment has provoked a deleterious effect on the corrosion behavior of the Al-9wt% Si alloy. In this particular case, such tendency of reduction on the corrosion resistance induced by the LSR process is associated with an increase of boundaries between the Al-rich (α) phase and Si particles that have dissimilar growth behaviors. The boundaries are imperfectly conformed due to a certain deformation in the atomic level, mainly on the Al-rich phase side of the interface, since Si grows from the melt in a faceted manner (smooth growth interface) while the α phase solidifies with surfaces that are rough. Such localized deformation induces an increase on the corrosion action for very fine microstructures (remelted samples). Recent studies [5, 12, 20, 24] dealing with the corrosion resistance of hypoeutectic Al-Si alloys have reported a similar result, i.e., with refined microstructures being connected to a decrease on the corrosion resistance. Fig. 6 shows microstructures illustrating tendencies for pitting corrosion for as-cast samples.

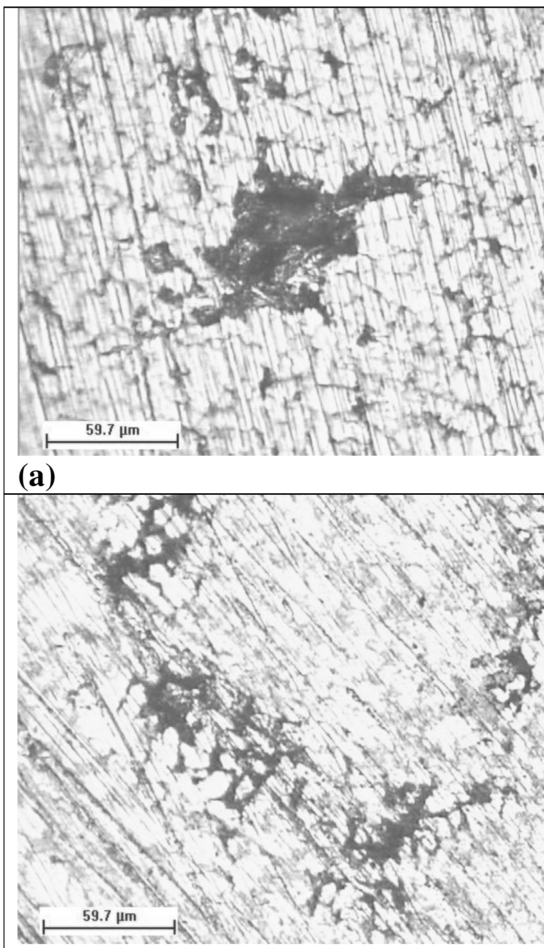

(a)

(b)

Figure 6. Typical microstructures of the Al-9wt%Si alloy: (a) as-cast with cooling rates from 2 to 4 ^{o}C/s and (b) as-cast with cooling rates: 8 to 12 ^{o}C/s after corrosion tests evidencing pitting corrosion.

4. CONCLUSIONS

The following main conclusions can be drawn from the present investigation:

(a) The laser surface remelting (LSR) has provided a significant microstructural refinement in an Al9wt%Si alloy sample compared to as-cast samples and has induced precipitation of silicon in the Al-rich matrix .

(b) The experimental corrosion tests results have shown that as-cast samples tend to yield higher corrosion resistance than laser remelted samples, and that this is associated with an increase of boundaries between the Al-rich (α) phase and Si particles in refined microstructures, since such boundaries are more susceptible to the corrosion action.

(c) Although the LSR has provided a displacement on the corrosion potential towards the nobler side, its corresponding corrosion current density increased about 2 times. However, the shapes of the cathodic and anodic branches of the as-cast Al-9wt% Si alloy sample characterize typical pitting reactions, differently to that exhibited for the laser remelted sample.

ACKNOWLEDGEMENTS
The authors acknowledge financial support provided by FAEPEX-UNICAMP, FAPESP (The Scientific Research Foundation of the State of São Paulo, Brazil) and CNPq (The Brazilian Research Council). The authors also thank Laboratório Nacional de Luz Sincrotron for permitting the use of laboratory facilities and Mr. Eli Wenzel de Siqueira for processing the samples in the laser machine.

References

1. N. J. Petch, *J. Iron Steel Inst.,* 174 (1953) 25
2. P. Donelan, *Mater. Sci. Technol*., 16 (2000)261
3. W. R. Osório, C. A. Santos, J.M.V. Quaresma, and A. Garcia, *J. Mater. Proc. Technol*., 143 (2003) 703
4. W. R. Osório, C. M. Freire, A. Garcia, *J. Alloys Compd.*, 397 (2005) 179
5. W. R. Osorio, N. Cheung, J.E. Spinelli, P. R. Goulart, and A. Garcia, *J. New Mater. Electrochem. Systems*, 11 (2008) 205
6. S.G. Shabestari and H. Moemeni, *J. Mat. Proc. Technol.* 153-4 (2004)193.
7. L. Heusler, and W.G. Schneider, *J. Light Metals*, 2, (2002) 17
8. A. Bokota, and S. Iskierka, *Acta Mater.,* 44 (1996) 445
9. N. Cheung, M.C.F. Ierardi, A. Garcia, and R. Vilar, *Lasers Eng.,* 10 (2000) 275
10. Y. Xianqing, Z. Chengjun, S. Xuefeng, H. Manping, and M. Jianguo, *Appl. Surf. Sci.,* 253 (2007) 4409.
11. W. Kurz, D. J. Fisher, *Fundamentals of Solidification*, Trans Tech Publications, Switzerland (1992).
12. W.R. Osório, N. Cheung, J.E. Spinelli, K.S. Cruz and A. Garcia. *Appl. Surf. Sci.,* 254 (2008) 2763
13. A. Munitz, *Metall. Trans*., 16B (1985) 149
14. M. Zimmermann, M. Carrard, and W. Kurz, *Acta Metall.*, 37 (1989) 3305
15. S. Virtanen, H. Böhni, R. Busin, T. Marchione, M. Pierantoni, and E. Blank, *Corr. Sci.* 36 (1994) 1625
16. B. K. Opera, V. M. Andriyakhin, V. I. Volgin, and V. V. Bandurkin, *Prot. Met*. 21 (1985) 74

17. T. T. Wong, and G. Y. Liang, *J. Mater. Proc. Technol.*, 63 (1997) 930
18. T. T. Wong, G. Y. Liang, and C. Y. Tang, *J. Mater. Proc. Technol.*, 66 (1997) 172
19. P. R. Goulart, W. R. Osório, J. E. Spinelli, A. Garcia, *Mater. Manufact. Proc.*, 22 (2007) 328.
20. W. R. Osório, P. R. Goulart, A. Garcia, Mater. Lett. 62 (2008) 365
21. M. M. Antonijevic, M. B. Petrovic, *Int. J. Electrochem. Sci.,* 3 (2008) 1127
22. B.M. Praveen,T.V. Venkatesha, *Int. J. Electrochem. Sci.,* 4 (2009) 267
23. W. R. Osório, J. E. Spinelli, C. M. Freire, A. Garcia, *Mater. Manufact. Proc.*, 22 (2007) 341
24. W. R. Osório, P. R. Goulart, G.A. Santos, C. Moura Neto, and A. Garcia, *Metall. Mater. Trans.*, 37A (2006) 2525
25. E. A. Noor, A. H. Al-Moubaraki, *Int. J. Electrochem. Sci.,* 3 (2008) 806
26. X. P. Niu, B.H. Hu, I. Pinwill, and H. Li, *J. Mater. Proc. Technol.*, 105 (2000) 119
27. S. A. Kori, B. S. Murty, and M. Chakraborty, *Mater. Sci. Eng.*, A 280 (2000) 58
28. E L. Rooy, *Aluminum and Aluminum Alloys.* Metals Park, OH: Castings: Metals Handbook; ASM International; (1988)